Orbital: The Electronic Journal of Chemistry
journal homepage: www.orbital.ufms.br
ISSN 1984-6428

| Vol 10 | | No. 1 | | Special Issue January 2018 |

Full Paper

Influence of Chromium (III) Insertion on the Thermal Stability of Carbonated Magnesium and Aluminum Hydrotalcites Synthesized by the Hydroxide Coprecipitation Method

Graciele Vieira Barbosa*[a], Jusinei Stropa Meirelles[b], Lincoln Carlos Silva de Oliveira[b], Rafael Aparecido Ciola Amoresi[c], Maria Aparecida Zaghete[c], Alberto Adriano Cavalheiro[a], Rogério Cesar de Lara da Silva[a]

[a]*LIMAN - CDTEQ - Universidade Estadual de Mato Grosso do Sul, R. Emílio Mascoli, 275 - Jardim Vale Encantado, 79950-000, Naviraí - MS, Brazil.*
[b]*INQUI - Universidade Federal de Mato Grosso do Sul, Av. Senador Filinto Muller, 1555 – Ipiranga, 79064-470, Campo Grande, MS, Brazil.*
[c]*LIEC - IQCar - Universidade Estadual Paulista, Rod. Araraquara-Jaú Km, Bairro Machados, 14800-901, Araraquara, SP, Brazil.*

Article history: Received: 30 June 2017; revised: 11 October 2017; accepted: 15 October 2017. Available online: 29 January 2018. DOI: http://dx.doi.org/10.17807/orbital.v10i1.1039

Abstract: Anionic clays are structures capable of adsorbing large quantities of water and other polar molecules in aqueous medium due to an ordered lamellar arrangement. Generally, the most stable composition contains magnesium and aluminum hydroxides, but other trivalent metal cations with similar ionic radii may also be inserted in co-substitution to the aluminum cation, targeting changes in the specificities of the adsorbed molecules, such as the chromium (III) one. The main objective of this work was to investigate the thermal stability of the carbonated magnesium-aluminum hydrotalcite when different amount of aluminium (III) cation is replaced by chromium (III) one. For that purposes, the hydrotalcite samples were obtained through the coprecipitation method at pH 11, followed by ageing stage at 80 °C, washing and drying at 100 °C for 24 h. The results obtained by thermal analysis, FTIR spectroscopy, and X-ray diffractometry techniques have permitted to conclude that chromium insertion leads to turbostratic disorder along the c-axis, which affects also the thermal stability and crystallinity of the precipitated materials. The chromium-based hydrotalcites showed to be more easily dehydrated at lower temperatures, with dependence predominantly kinetic, which leads to significant volume contraction and the hindering of the subsequent dehydroxylation stage at higher temperatures.

Keywords: chromium (III); hydrotalcite; precipitation; thermal analysis; X-ray diffraction

1. INTRODUCTION

The hydrotalcite compounds are anionic clays material type with lamellar double hydroxide structure containing Pearson's hard acid, such as Mg^{+2}, Zn^{+2} or Co^{+2}, co-substituted by trivalent ones, such as Al^{+3}, Cr^{+3} or Fe^{+3}, in order to generate an excess of stable positive charges in the lamellae. That charge imbalance is neutralized by adsorption of several interlamellar species, like the carbonate ion CO_3^{-2} [1-3]. In general, the carbonated structures of magnesium and aluminum hydrotalcites have the composition described nominally by $Mg^{+2}_{(1-x)}Al^{+3}_x(OH^-)_2(CO_3^{-2})_{x/2}.yH_2O$, where the value of x must be between 0.67 and 0.8, so that the structure exhibits a minimum of thermal stability [4-8].

The carbonated hydrotalcites of magnesium and aluminum crystallizes as a rhombohedral structure R-3m, in a complex cross-linked bond structure, where the lamellae octahedrons are shared by its vertices in two-dimension. The tridimensional structure emerges when interlamellar species, like water and carbonate ions form bridge bonds among the lamellae in c-axis direction, give it a long range ordering [9-13].

Nevertheless, that common hydrotalcite composition based on magnesium and aluminum can be modified very precisely both in their cationic and anionic sites. In general, the trivalent transition metal

*Corresponding author. E-mail: grace.navi.21@gmail.com

cations can be inserted in co-replacement to aluminum III, such as chromium III, iron III and scandium III. That substitution approach keeps unaltered the positive charges excess on the lamellae, but can changes the crystallinity, the adsorptive characteristics, and the thermal stability for dehydration, dehydroxylation, and decarbonation processes [14-20].

Hydrotalcite-like compounds are applied as numerous biomedical applications, such as cosmetics, biosensing, and gene or drug deliveries. Hydrotalcite nanoparticles have been successfully applied for the delivery of anticancer drugs in tumor cells and the distribution of hydrotalcite nanoparticles in several human organs, as liver, kidney and spleen, well as in lung at slight occurrence was also investigated. Hydrotalcite nanoparticles toxicity was found to be lower than other inorganic nanoparticles and showed also no accumulative behavior due the easy dissolution in body fluid in dosages typically used for biomedical applications. Nevertheless, there is a strong dependence of the composition and average particle size, which makes the proposition and investigation of new compositions for hydrotalcite structures an important step before their use as drug delivery [21-23].

Taking into account the chemistry of solution for synthesizing the hydrotalcite samples by coprecipitation method, it is possible to observe the several hydrate transition metal cations affect the homogenization and the crystallization process due the consistent difference among the solubility products for their isolated hydroxide precipitates. Some of them can be very difficult to obtain, like the chromium modified ones, due the high stability of hexahydrate chromium (III) complex. Thus, a digestion step is often carried out after the precipitation in order to promote a structural homogenization [24-28]. In spite of that characteristic, new compositions can be good catalysts or ion exchanger material in various fields, mainly in environmental sciences [29-34].

It was previously demonstrated that carbonated magnesium aluminum hydrotalcites can be satisfactorily structured as nanoparticles by replacing the aluminum cation by chromium trivalent one and was also proved its ability to incorporate organic and inorganic anions through ion exchange or hydrothermal treatment. However, some of the physic-chemical properties for trivalent chromium hexahydrate cations harms the ordering process and low crystalline structures were found for chromium-based double hydroxide compositions due the higher mismatch along the perpendicular direction of the lamellae planes [33,34]. Under the viewpoint of the biomedical applications, it was also demonstrated the cell membrane cannot uptake species with chromium (III), like the aquocomplexes or other metalocompound with chromium(III) and so toxicity of the chromium(III)-containing materials was not observed [35].

In order to investigate some aspects of chromium (III) modified hydrotalcites, like the dehydration, dehydroxylation, and decarbonation processes, and to understand some effects on the crystallinity and thermal stability of the samples, three compositions of carbonated hydrotalcite of magnesium and aluminum co-substituted with chromium (III) were prepared through the hydroxide precipitation method at pH 11.

2. MATERIAL AND METHODS

All of the carbonated hydrotalcite samples were synthesized by using analytical grade reagents based on aqueous soluble salts hexahydrate magnesium II nitrate $Mg(NO_3)_2.6H_2O$, nonahydrate aluminum III nitrate $Al(NO_3)_3.9H_2O$, and nonahydrate chromium III nitrate $Cr(NO_3)_3.9H_2O$. The batches of magnesium-aluminum-chromium mixed cation solutions were prepared by simultaneous dissolution of those aqueous soluble salts in distilled water at room temperature.

Besides that, the batches of hydroxide-carbonate mixed precipitating anions were prepared by simultaneous dissolution of sodium hydroxide NaOH and sodium carbonate Na_2CO_3 with distilled water and at room temperature too. The content of each cation-anion solution pair flask was poured on a third one in order to promote the co-precipitation of each hydrotalcite sample under vigorous stirring, yielding very stable suspension. The molar cation ratio was controlled by x value, set as 0, 0.1, and 0.2, according to the general formula by $Mg^{+2}_{0.7}Al^{+3}_{0.3-x}Cr^{+3}_{x}(OH^{-})_2(CO_3^{-2})_{0.15}$.

The precipitate samples were named according to the composition, where the HTM7A3C0 sample (x = 0) represents the $Mg_{0.7}Al_{0.3}(OH)_2(CO_3)_{0.15}$ nominal composition, the HTM7A2C1 (x = 0.1) and HTM7A1C2 samples (x = 0.2) represent the $Mg_{0.7}Al_{0.2}Cr_{0.1}(OH)_2(CO_3)_{0.15}$ and $Mg_{0.7}Al_{0.1}Cr_{0.2}(OH)_2(CO_3)_{0.15}$ nominal compositions,

respectively. The obtained precipitate samples was lead to the ageing stage at 80 ºC for 6 hours under slow stirring, and left to stand overnight.

In order to purify the precipitate samples, each precipitate was filtered several times with distilled water until the waste water reaches neutral pH. Then, the washed precipitate was dried at 85 °C for 24 hours in a drying oven, slightly crushed in a porcelain mortar, re-dried again at 100 °C for 24 hours and lead to the characterization by Thermal Analysis (simultaneous TG/DSC) in Netszch - Thermische Analyze equipment (TASC 414/2 controller and Pt 10 thermocouple), heated at 10 ºC min^{-1} under synthetic air flow of 30 cc min^{-1}.

The sample materials were characterized by X-ray diffraction in Siemens D5005equipment (K-alpha-Cu), where the observed reflections were identified through JCPDS database [36]. Finally, the samples were observed through Fourier Transform Infrared Spectrometry (FTIR) in Nexus 650 Thermo Nicolet equipped with photoacoustic detector, where the main functional groups were identified according the literature [37].

3. RESULTS AND DISCUSSION

The weight losses (TG) of each thermal event followed by their first derivative (DTG) and calorimetric (DSC) curves were used to determine several parameters associated to the drying, dehydration, dehydroxylation and decarbonation processes occurring in each hydrotalcite precipitate sample dried at 100 ºC for 24 hours. Those results are compiled in Table 1 and the original curves are shown in Figure 1.

Based on the DTG peaks it was proposed a set of temperature range taking into account the subsequent decomposition processes. The dehydration seems to occur in two stages (I and II), probably due the energetic differences between external and interlamelar adsorbed water molecules. However, with the chromium content increasing, the external water is 100 % higher for HTM7A1C2 sample (14.4 %) if compared to HTM7A3C0 one (7.7 %), while an inverse behavior is observed for interlamelar water (II). These aspects can be observed by the flattening of DTG and DSC curves in that temperature range, mainly up to 250 ºC. The chromium insertion seems to displace the drying process to lower temperatures, below 100 ºC, which permits to concludes the drying process has a kinetic character [38] and was not finalized during the drying stage at 100 ºC for 24 hours.

The dehydroxylation stages (III and IV) present opposite behavior if compared to I and II ones, because the second stage dehydroxylation (IV) becomes wider and more pronounced as a function of the chromium content increasing, overlapping the stage III. It is very probable the dehydration stages at lower temperatures (I and II) have strong correlation with dehydroxylation ones (III and IV).

Thus, during the dehydration process, the lamellae are sintered through the formation of cross-linked bonds, hindering the dehydroxylation, because the large amount of hydroxyl groups becomes interlamelar. In fact, during the sample preparation, a pronounced volume contraction in dehydration stage at 100 ºC has been often observed for chromium-based hydrotalcites. In addition, that volume contraction seems to be correlated with carbonate amount, because a less carbonated hydrotalcite has less anchorage between the lamellas.

Table 1. Thermal events for carbonated magnesium-aluminum hydrotalcite dried at 100ºC for 24 h.

Thermal event	Temperature range ºC	Weight loss determined for each sample (%)		
		HTM7A3C0	HTM7A2C1	HTM7A1C2
I - External dehydration	30 - 180	7.7	14.1	14.4
II – Interlamelar dehydration	180 - 250	8.7	3.5	2.1
III - External dehydroxylation	250 - 350	10.1	7.8	7.5
IV - Interlamelar dehydroxylation	350 - 420	9.8	13.9	13.9
V - Decarbonation	420 - 900	8.0	5.8	5.8
Final residue at 900 ºC		55.7	54.9	56.3

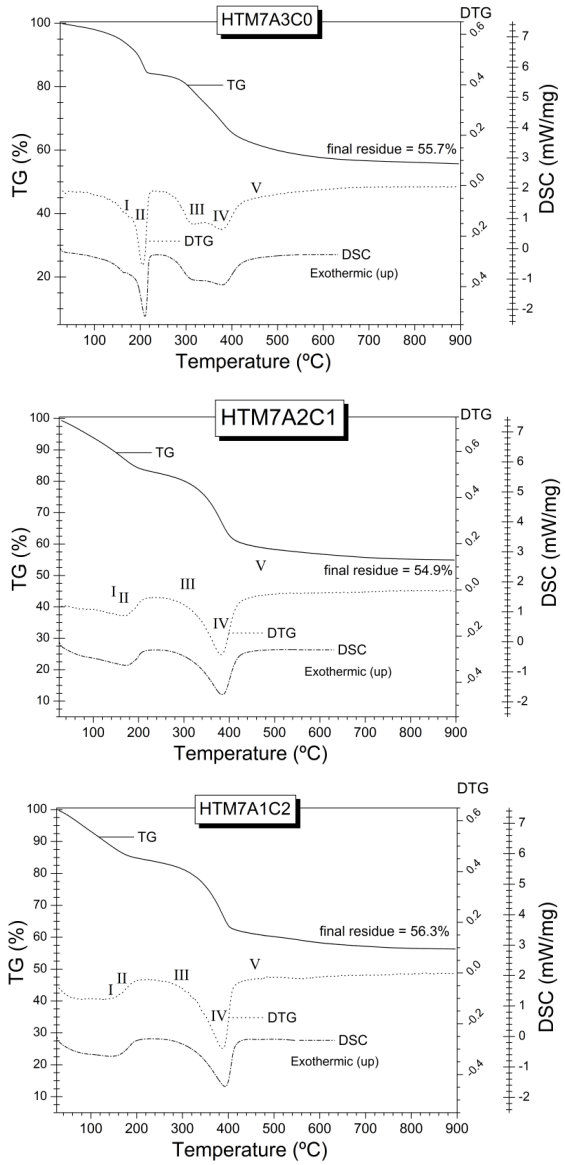

Figure 1. Thermal analysis (TG/DTG/DSC) for carbonated magnesium-aluminum hydrotalcite dried at 100ºC for 24 hours, as a function of chromium content: a) HTM7A3C0, b) HTM7A2C1 and c) HTM7A1C2 samples.

FTIR spectra can aid to understand the influences observed in thermal analysis and are shown in Figure 2. The bands at 3500 cm^{-1} (I) and at 3000 cm^{-1} (II) are related to the stretching vibration of -OH groups from interlayer water and metal hydroxides, respectively. In spite of the appearing the CO_2 band at 2350 cm^{-1} (III) and the set of bands at 1650 cm^{-1} (IV), at 1540 cm^{-1} (V), and at 1360 cm^{-1} (VI) refers to vibration of interlayer hydrated carbonate ions, mainly the VI band, which sharper band is related to carbonate anions electrostatically to in the interlayer space due larger amount of water interlayer acting as solvent [30].

The hydroxide layer structure give origin to other set of bands signaled as VIII, which is related to the M1-O-M2 vibration modes, strongly influenced by global crystal structure. Thus, chromium-based hydrotalcites seems to have a less ordered layer-interlayer structure due less intense bands and the strong overlapping of the bands at lower wavelength (VIII), which are directly related to the crystalline ordering, as can be view also by X-ray diffraction patterns for these samples (Figure 3).

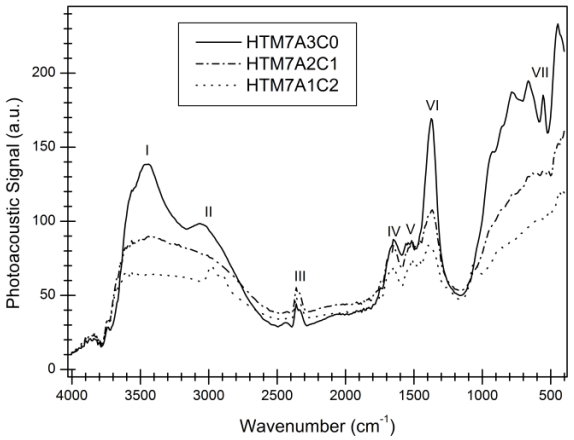

Figure 2. FTIR spectra for carbonated magnesium-aluminum hydrotalcite dried at 100ºC, as a function of chromium content.

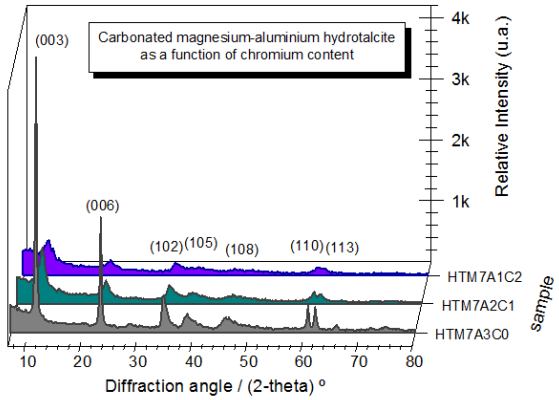

Figure 3. X-ray diffraction patterns for hydrotalcite samples dried at 100ºC for 24 hours, as a function of chromium content.

In spite of the X-ray diffraction patterns for all samples to be related to LDH structure with R-3m rhombohedral symmetry, according JCPDS card number 89-5434 and no residual nitratine $NaNO_3$ phase (JCPDS card number 89-2828) was found, which implicates the washing stage was successfully carried out for all of the samples. It is possible the

occurrence of another structure based on magnesium-chromium hydroxide carbonate, maybe with low crystallinity, like the stichtita $Mg_{0.75}Cr_{0.25}(CO_3)_{0.125}(OH)_2(H_2O)_{0.5}$, which possess also a R-3m rhombohedral symmetry, according JCPDS card number 45-1475. The carbonated magnesium-aluminum hydrotalcite has all of the X-ray diffraction peaks matching with the magnesium-chromium hydroxide carbonate stichtita ones, so that it is not possible to differentiate them in this case.

Regardless of whether the secondary phase of stichtita is present or not in samples containing chromium, there are clear differences in the crystallinity among the samples as a function of chromium content, corroborating the results observed by FTIR spectra. All of the (*h k l*) reflections for R-3m rhombohedral hydrotalcite undergo the intensity decreasing for chromium-based compositions, if compared to no chromium modified sample HTM7A3C0. However, between HTM7A2C1 and HTM7A1C2 samples, no significant decreasing in (*h k l*) reflections can be observed. By considering only the (0 0 *l*) reflections, such as the (0 0 3) and (0 0 6) ones, at 12 and 22 º(2-theta) degrees, respectively, then the effect of chromium insertion on the c-axis ordering can be understood, because the observed decreasing for these (0 0 *l*) reflections are more pronounced than (1 *k l*) ones, related to a,b axes.

Taking into account these results obtained by x-ray diffraction, which are corroborated by FTIR spectra and thermal analysis, it is possible to infer the c-axis reflections undergo turbostratic disorder, leading to the layers disorientation about the c axis, as well described in previous work [34]. In Figure 4 is shown an illustration to help understand that turbostratic disorder in terms of layers arrangement along the c-axis, which is changed as a function of the chromium content. Maybe, the lower amount of carbonate interlayer is the cause for that behavior, which seems to be dependent of chromium content. That behavior seems to be present even in the drying stage carried out at 100 ºC for 24 hours.

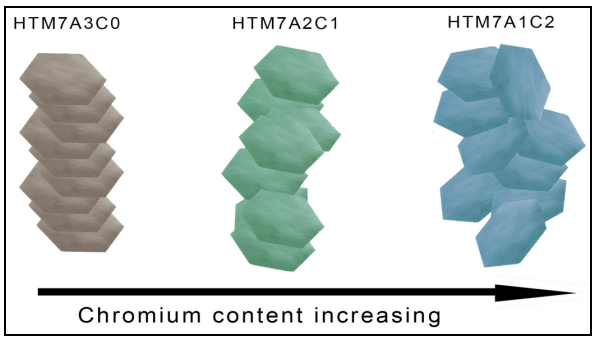

Figure 4. Illustration for proposed c-axis disorder into carbonated magnesium aluminum hydrotalcites dried at 100ºC for 24 hours, as function of chromium content.

4. CONCLUSION

Carbonated magnesium-aluminum hydrotalcites were synthesized through the coprecipitation method at pH 1, followed by ageing at 80 ºC for 6 hours. All of the samples were fully characterized by thermal analysis, FTIR spectroscopy and X-ray diffractometry techniques, which have permitted to conclude that chromium insertion leads to turbostratic disorder along the c-axis, with severe consequences for the thermal stability and crystallinity. Less carbonated structure was found for chromium-based hydrotalcites, which eases the dehydration stage, leading to accentuated volume contraction and the hindering of the subsequent dehydroxylation stage at higher temperatures. Thus, as consequence, the dehydroxylation is hindered and the material becomes structurally more stable, which makes a potential drug delivery, mainly taking into account the acidic characteristics for several molecules.

5. ACKNOWLEDGMENTS

The authors thank FUNDECT-MS, CNPq, CAPES and FINEP for financial supports.

6. REFERENCES AND NOTES

[1] Belloto, M.; Rebours, B.; Clause, O.; Lynch, J.; Bazin, J. L. D.; Elkaïn, E. *J. Phys. Chem.* **1996**, *100*, 8535. [CrossRef]

[2] Setshedi, K.; Reni, J.; Aoyi, O.; Onyango, M. S. *Int. J. Phys. Sci*. **2012**, *7*, 63. [CrossRef]

[3] Debek, R.; Motak, M.; Grzybek, T.; Galvez, M. E.; Da Costa, P. *Catalysts* **2017**, *7*, 32. [CrossRef]

[4] Shen, J.; Kobe, J. M.; Chen, Y.; Dumesic, J. A. *Langmuir* **1994**, *10*, 3902. [CrossRef]

[5] Baskaran, T.; Christopherb, J.; Sakthivel, A. *RSC Adv.* **2015**, *5*, 98853. [CrossRef]

[6] Sani, T.; Gómez-Hortiguela, L.; Pérez-Pariente, J.; Chebude, Y.; Díaz, I. *Sep. Purif. Technol.* **2015**, *157*, 241. [CrossRef]

[7] Hafshah, H.; Prajitno, D. H.; Roesyadi, A. *J. Pure App. Chem. Res.* **2016**, *5*, 182. [CrossRef]

[8] Wiyantokoa, B.; Kurniawatia, P.; Purbaningtiasa, T. E.; Fatimah, I. *Procedia Chem.* **2015**, *17*, 21. [CrossRef]

[9] Shekoohi, K.; Hosseini, F. S.; Haghighi, A. H.; Sahrayian,

A. *MethodsX* **2017**, *4*, 86. [CrossRef]

[10] Fahami, A.; Beall, G. W. *Mater. Lett.* **2016**, *165*, 192. [CrossRef]

[11] Rodilla, J. M.; Neves, P. P.; Pombala, S.; Rives, V.; Trujillano, R.; Díezc, D. *Nat. Prod. Res.* **2015**, *30*, 834. [CrossRef]

[12] Obalová, L.; Jirátová, K.; Kovanda, F.; Pacultová, K.; Lacný, Z.; Mikulova, Z. *Appl. Catal., B* **2005**, *60*, 289. [CrossRef]

[13] Tsai, T.-Y.; Laiob, J.-R.; Naveen, B.; Wu, T.-C. *J. Chin. Chem. Soc*. **2017**, *64*, 851. [CrossRef]

[14] Debek, R.; Motak, M.; Galvez, M. E.; Da Costa, P.; Grzybek, T. *Reac. Kinet. Mech. Cat.* **2017**, *121*, 185. [CrossRef]

[15] Wang, J.; Xu, A.; Jia, M.; Bai, S.; Chenga, X.; Zhaorigetu, B. *New J. Chem*. **2017**, *41*, 1905. [CrossRef]

[16] Yang, T.; Zhang, X.-Y.; Zhang, X.-X.; Chen, M.-L.; Wang, J.-H. *ACS Appl. Mater. Interfaces* **2015**, *7*, 21287. [CrossRef]

[17] Mao, N.; Zhoua, C. H.; Tonga, D. S.; Yua, W. H.; Lin, C. X. C. *Appl. Clay Sci.* **2017**, *144*, 60. [CrossRef]

[18] Deng, L.; Shi, Z.; Li, B.; Yang, L.; Luo, L.; Yang, X. *Ind. Eng. Chem. Res.* **2014**, *53*, 7746. [CrossRef]

[19] Pérez, E.; Ayele, L.; Mayoral, A.; Getachew, G.; Fetter, G.; Bosch, P.; Diaz, I. *J. Environ. Chem. Eng.* **2015**, *3*, 1555. [CrossRef]

[20] Wu, G.; Wang, X.; Li, J.; Zhao, N.; Wei, W.; Sun, Y. *Catal. Today* **2008**, *131*, 402. [CrossRef]

[21] Carpentier, J.; Siffert, S.; Lamonier, J.F.; Laversin, H.; Aboukais, A. *J. Porous Mater.* **2007**, *14*, 103. [CrossRef]

[22] Choi, S.-J.; Choy, J.-H. *Nanomedicine* **2011**, *6*, 803. [CrossRef]

[23] Bi, X.; Zhang, H.; Dou, L. *Pharmaceutics* **2014**, *6*, 298. [CrossRef]

[24] Rossi, T. M.; Campo, J. C.; Souza, M. M. V. M. *Adsorption* **2015**, *22*, 151. [CrossRef]

[25] Tamura, H.; Chiba, J.; Ito, M.; Takeda, T.; Kikkawa, S.; Mawatari, Y.; Tabata, M. *J. Colloid Interface Sci.* **2006**, *300*, 648. [CrossRef]

[26] Cocheci, L.; Barvinschi, P.; Pode, R.; Popovici, E.; Seftel, E. M. *Chem. Bull. "POLITEHNICA" Univ. (Timisoara)* **2010**, *55*, 40. [Link]

[27] Daza, C. E.; Cabrera, C. R.; Moreno, S.; Molina, R. *Appl. Catal., A* **2010**, *378*, 125. [CrossRef]

[28] Basag, S.; Kovanda, F.; Piwowarska, Z.; Kowalczyk, A.; Pamin, K.; Chmielarz, L. *J. Therm. Anal. Calorim.* **2017**, *129*, 1301. [CrossRef]

[29] Lia, Y.; Gaoa, B.; Wub, T.; Sunb, D.; Lia, X.; Wanga, B.; Lu, F. *Water Res.* **2009**, *43*, 3067. [CrossRef]

[30] Labajos, F. M.; Rives, V. *Adv. Inorg. Chem.* **1996**, *34*, 5313. [CrossRef]

[31] Kameda, T.; Yabuuchi, F.; Yoshioka, T.; Uchida, M.; Okuwaki, A. *Water Res.* **2003**, *37*, 1545. [CrossRef]

[32] Yang, C.; Liao, L.; Lv, G.; Wu, L.; Mei, L.; Li, Z. *J. Colloid Interface Sci.* **2016**, *479*, 115. [CrossRef]

[33] Saifullah, B.; Hussein, M. Z. B. *Int. J. Nanomedicine.* **2015**, *10,* 5609. [CrossRef]

[34] Prakash, A. S.; Kamath, V.; Hegde, M. S. *Mater. Res. Bull.* **2000**, *35*, 2189. [CrossRef]

[35] Cohen, M. D.; Kargacin, B.; Klein, C. B.; Costa, M. *Crit. Rev. Toxicol.* **1993**, *23*, 255. [CrossRef]

[36] JCPDS - Joint Committee on Powder Diffraction Standards/International Center for Diffraction Data, Pennsylvania, Powder Diffraction File 2003.

[37] Socrates, G. Infrared and Raman Characteristic Group frequencies, 3th ed., John Wiley & Sons: Chichester, 2004. [Link]

[38] Rhee, S. W.; Kang, M. J. *Korean J. Chem. Eng.* **2002**, *19*, 653. [CrossRef]